Spatially Variant Resolution Modelling for Iterative List-Mode PET Reconstruction

Matthew G. Bickell, Lin Zhou, Johan Nuyts

***Abstract*—A spatially variant resolution modelling technique is presented which estimates the system matrix on-the-fly. The method randomly redistributes the line-of-response endpoints according to probability density functions describing the detector response and photon acollinearity effects. A list-mode OSEM algorithm is used for the reconstruction. We demonstrate that this model agrees with measured PSFs and we present results showing an improvement in resolution recovery as compared to using a Gaussian convolution to model the resolution, although with an increase in noise. We also present results from applying this method to event-by-event rigid motion correction with list-mode reconstruction using the microPET Focus220 scanner.**

I. Introduction

In positron emission tomography (PET) imaging accurately modelling the physical measurement process to account for the point spread function (PSF) can improve the subsequent resolution of the reconstruction [1]. Such a model can be used to calculate a system matrix which represents the mapping between the detector elements and the voxels in the image space. This system matrix can be determined directly from point sources measurements throughout the scanner field-of-view [2], estimated using, for example, Monte Carlo simulations [3], or determined analytically [4].

During maximum likelihood expectation-maximisation (MLEM) iterative reconstruction the modelling of the finite spatial resolution may be accomplished by convolving the image with a suitable Gaussian distribution before forward projection and after backprojection [5]. The projections can be performed using, for example, a ray-tracing technique [6]. This Gaussian distribution is spatially invariant and is only an accurate model for the resolution near the centre of the field-of-view (FOV) of the PET scanner; it becomes less accurate with increasing radial distance.

In this work a spatially variant model has been developed which models the two most dominant factors affecting the PSF, namely the detector response function and the acollinearity of the photon pair, for the microPET Focus220 small animal scanner. Probability density functions (PDFs) are derived which represent the statistical distribution of where the photons were absorbed in the crystals. These PDFs are randomly sampled to define the endpoints of the lines-of-response (LORs), thus redistributing them and modelling the system's response (this is an extension of earlier work [7]). A list-mode ordered-subset expectation maximisation (OSEM) reconstruction is then performed [8].

M. G. Bickell, L. Zhou, and J. Nuyts are with the Medical Imaging Research Centre, Department of Nuclear Medicine, KU Leuven, Belgium.

This work is supported by the IMIR project of KU Leuven.

Similar techniques have been employed before in various ways to model the system matrix [9]–[14]. Moehrs *et al* [9] used multiple integrations of each LOR to achieve an approximation of the system matrix; Chen *et al* [10] presented an approach whereby the PDFs were estimated from Monte Carlo simulations, and applied the algorithm to simulated data. A random redistribution methodology was applied by Jin *et al* [11] to reassign LORs which had undergone mashing when being binned to a sinogram. This was done by randomly assigning sinogram bin elements to those LORs which could have contributed to that bin, weighted by their relative sensitivities. While this does involve a redistribution, the goal was not to model the physical processes involved in the measurement, but rather to model the PSF due to mashed data.

Rigid motion correction in PET brain imaging is becoming more and more important with the currently achievable resolution of modern scanners. The most successful motion correction techniques make use of an external motion tracker during the scan to track either a marker fixed to the subject [16], [17] or characteristic features of the subject itself (i.e. markerless tracking) [18], [19]. The list-mode data can then be corrected on an event-by-event basis according to the recorded motion data before reconstruction [16]. For subjects which may exhibit a large range of motion within the scanner (for instance, awake animals in pre-clinical studies), the need to respect the spatially variant nature of the system matrix becomes more important. The presented resolution modelling technique allows for the system model to be incorporated before motion correction is performed, thus preserving the spatially variant nature of the model and providing a more accurate system model than spatially invariant techniques.

II. The measurement process

During the decay of the radioisotope a positron is emitted. This positron can traverse some distance (referred to as the positron range) before annihilating with an electron. The positron range is dependent on the surrounding material as well as the energy of the positron and varies for different tracers.

The linear momentum of the electron and positron is conserved in the annihilation event, thus the emitted photon pair can have a non-zero linear momentum and hence have acollinear directions of travel. In this case the resultant LOR connecting the detecting crystals will not pass through the location of the annihilation event, thus introducing a blurring in the reconstructed image. The magnitude of this blurring depends on the length of the photons' flight path and is thus spatially variant.

Due to the finite stopping power of the scintillation crystals a photon with an oblique incident angle on the crystal surface

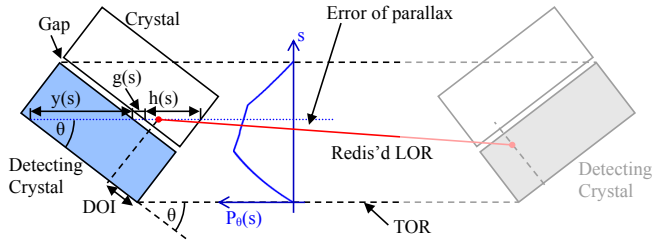

Fig. 1. The detector response function, $P_\theta(s)$, gives the probability that, given a detecting crystal pair which describe an incident angle θ, the photon was actually absorbed at s, a distance parameter perpendicular to the TOR. An independent sampling from $P_\theta(s)$ is made for each LOR endpoint.

might traverse one or more crystals before being absorbed. The recorded position of the detection event is the centre of the detecting crystal, and hence, even for photons whose flight is normal to the crystal, an uncertainty of half the crystal width is introduced. Furthermore, photon scatter within the crystal can cause it to be absorbed in a neighbouring crystal, and imperfect optical septa between the scintillation crystals can cause crosstalk between them. These effects result in a detector response function which depends primarily on the incident angle of the photon on the crystal surface.

III. Method

By analytically modelling the physical factors affecting the measurement process, suitable PDFs can be derived which represent the statistical location of the absorption points of the photons in the detecting crystals. Thus, given a detecting crystal pair, a LOR can be defined by randomly selecting endpoints according to these PDFs. This "redistributed" LOR can then be considered to be a single line sample from the tube-of-response (TOR) connecting the crystals.

Since any particular detecting pair appears many times in the list-mode data, by redistributing all the LORs independently the TOR corresponding to each detecting pair is sufficiently sampled, given a high enough number of counts. Thus the complete system matrix is suitably estimated.

A. Modelling the measurement process

1) Detector response function: A photon entering a crystal traverses some distance before being absorbed. The probability distribution of a photon being absorbed by a crystal when it is at a perpendicular distance of s from the TOR edge which makes an angle of θ with the crystal normal, is given by,

$$P_\theta(s) = \left(1 - e^{-\mu_c y(s)}\right) e^{-\mu_c h(s) - \mu_g g(s)}, \qquad (1)$$

where $h(s)$ is the distance traversed in the neighbouring crystals, $y(s)$ is the total potential distance traversed in the crystal under consideration, $g(s)$ is the distance traversed through the gaps between the crystals, and μ_c and μ_g are the attenuation coefficients of the crystals and the material filling the gaps between the crystals, respectively, [20]–[22]; see figure 1. The parallax effect which varies the incident angle, θ, across the distribution, $P_\theta(s)$, has been ignored since the width of $P_\theta(s)$ is very small in comparison to the distance between the two detecting crystals. This models the depth of interaction of the crystal and accounts for the obliqueness of the crystal with LORs at increasing radial distance from the centre, but ignores the crystal scatter and crosstalk effects. These, and any additional physical effects which have not been included in the model, can be incorporated through a convolution with a suitable Gaussian distribution. The FWHM of this Gaussian was determined by comparison with measured data, and is discussed further in section IV-A.

The endpoints of each LOR are redistributed by randomly sampling from $P_\theta(s)$ twice: once for each endpoint, to define a redistributed LOR.

2) Photon acollinearity: Due to the conservation of electron-positron momentum, two photons emitted from an annihilation event are not exactly collinear. The distribution of the angular deviation of this acollinearity was measured by Colombino *et al* [23] and later quantified by Shibuya *et al* [24]. The required distribution to describe this deviation was found to be a double Gaussian,

$$Q(\phi) = A_1 e^{-\frac{(\phi-\mu_1)^2}{2\sigma_1^2}} + A_2 e^{-\frac{(\phi-\mu_2)^2}{2\sigma_2^2}}, \qquad (2)$$

with $A_1 = 0.824$, $\sigma_1 = 0.269°$, $\mu_1 = -0.009°$, $A_2 = 0.176$, $\sigma_2 = 0.116°$ and $\mu_2 = 0.007°$ [24]. However, since there is no physical reason why the μ values should be non-zero, these can be set to zero.

Given an angular distribution, $\langle\phi\rangle$, between the travelling lines of the two photons, the resultant spatial distribution, $\langle p\rangle$, on a perpendicular plane at a distance d from the annihilation point is given by,

$$\langle p\rangle = d\tan\langle\phi\rangle. \qquad (3)$$

Extending equation 3 to allow for the orientation and curvature of the detecting surface, a distribution is derived with which the endpoint of the LOR can be redistributed.

The annihilation location distribution due to acollinearity can be approximated in two ways: either by redistributing one endpoint of the LOR, but selecting which at random; or by redistributing both LORs independently after scaling the standard deviations of the acollinearity distribution by $\frac{1}{\sqrt{2}}$. The former case can be thought of as considering one photon to be along the "true" flight path while the other has deviated from it by an angle of ϕ, and the latter case is where both photons are considered to have deviated from the "true" flight path by an angle of $\frac{\phi}{2}$. A comparison between the resultant distributions for these two cases with the theoretical distribution is shown in figure 2. Shifting only one endpoint provides a better approximation to the theoretical prediction. While in the regions close to the LOR endpoints this distribution has much higher values than the theoretical distribution, these regions are usually outside of the FOV of the scanner and are thus not as significant as the region around the centre of the FOV.

3) Positron Range: The positron range can be modelled by,

$$R(x) = Ae^{-x/B} + (1-A)e^{-x/C}, \qquad (4)$$

where, for ^{18}F in water, $A = 0.851$, $B = 0.054$ mm and $C = 0.254$ mm, and were set experimentally [25]. Since this

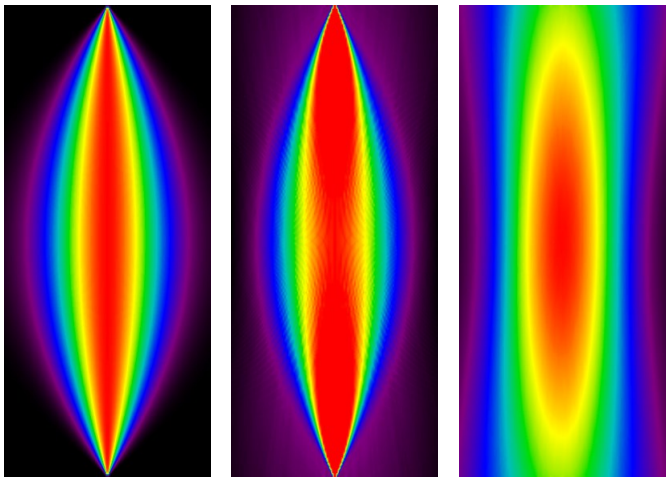

Fig. 2. The theoretical distribution of the possible annihilation points for a given LOR (along the vertical centreline) as a result of photon acollinearity is shown on the left. The resultant distributions when shifting only one LOR endpoint (middle) and when shifting both endpoints (right) are shown for comparison. The horizontal axis has been greatly exaggerated: actual spatial extents are 1.5 mm $\times$ 272 mm.

function already becomes very small when $x = \pm 1.0$ mm, its effect on the reconstruction is minimal and it was thus ignored during this research (unless explicitly specified).

B. Implementation

The above techniques were applied to model the system response of the microPET Focus220 (Preclinical Solutions, Siemens Healthcare Molecular Imaging, Knoxville, TN, USA).

1) Reconstruction: Before reconstruction all the LOR endpoints are redistributed independently according to the distributions described above; first according to the detector response function, and then according to the acollinearity distribution, in both the transaxial and axial directions. The LORs are sampled twice: once for the forward projection and once for the backprojection step in the MLEM algorithm. These two samplings are independent of each other. After each iteration the LORs are resampled so as to yield better statistics of the distributions. Thus, if a particular LOR appears N times in the list-mode data and the OSEM reconstruction is performed using M iterations, the corresponding TOR is sampled $2NM$ times during the reconstruction.

2) Normalisation: A normalisation measurement was made by scanning a uniform cylinder over a long period. To produce the sensitivity image used in the list-mode reconstruction the normalisation sinogram was inverted and backprojected. Before backprojection the LORs were redistributed according to the technique described in section III-A. This process was repeated $N = 25$ times to ensure that the distributions were well sampled, and the final sensitivity image was scaled by N.

IV. Experiments

All experiments were performed on the microPET Focus220 scanner. This is a specialised scanner dedicated to small animal imaging. It has a ring diameter of 260 mm and an axial length of 76 mm.

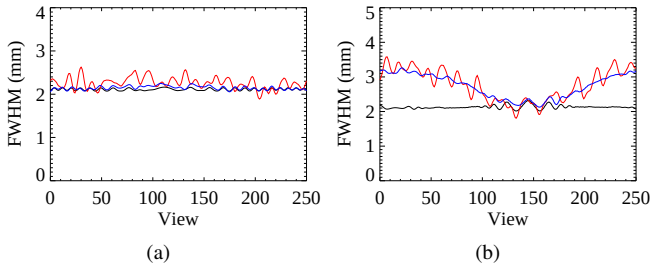

Fig. 3. The FWHM of the projection as a function of projection angle (view) in: the measured sinogram (red), the sinogram produced when using a Gaussian convolution to model the resolution (model A, black), and the sinogram produced when using the redistribution technique to model the resolution (model B, blue). In figure (b) the particle was located 1.694 cm from the centre of the field-of-view. To produce these plots the sinogram planes were summed over to reduce the effect of noise, and the plots have also been smoothed. The FWHM values have been arc-corrected. The redistribution technique produces sinograms whose projection profiles match those of measured data.

A. Spatial Variance Investigation

To investigate the spatially variant nature of the redistribution technique, a 2 mm diameter point source was scanned at various locations within the scanner. For each measurement the centre-of-mass position of the point source was determined from a reconstruction of the data, a point source of the same size was then simulated in that position and used to create a sinogram using two forward projection models:

- A The resolution was modelled by convolving the image with a spatially invariant Gaussian distribution with FWHM = 1.3 mm [26]. The resulting image was then forward projected to sinogram space.
- B The resolution was modelled by redistributing the LORs according the technique described above, forward projecting along these LORs, and then binning the resulting projection values into the sinogram bins corresponding to the original LORs.

The resulting sinograms were compared to the measured sinogram to determine the accuracy of each model in approximating the PSF.

B. Static phantom scans

A hot-rod phantom with rods of diameter 1.5 - 3.0 mm was scanned. Two scans were performed: one with the phantom near the centre of the FOV, and the other with the phantom approximately 5.4 cm horizontally to the left of the FOV centre. The phantom was filled with 1 mCi of ^{18}F-FDG and scanned for 2 minutes in each position. The reconstructions have a pixel size of $[0.4745, 0.4745, 0.7960]$ mm and were reconstructed with OSEM using 10 iterations with 10 subsets.

C. Moving phantom scan

The same hot-rod phantom, filled with approximately 1 mCi of ^{18}F-FDG, was scanned while undergoing a continuous

No resolution modelling Redistribution technique Gaussian convolution

Fig. 4. Reconstructions of the phantom near the centre of the scanner FOV. The redistribution technique has produced a similar resolution recovery to the Gaussian convolution technique, although with an increase in noise.

motion. The average radial distance of the phantom from the FOV centre during the scan was 3.8 cm. Its motion was tracked by attaching a marker to the phantom and tracking this marker with a MicronTracker stereo-optical camera (Claron Technology Inc., Toronto, Canada). The redistribution technique was applied to the list-mode data, and the list-mode data was then corrected for motion on an event-by-event basis [16], [17]. The data was reconstructed using a list-mode OSEM algorithm with 10 iterations and 10 subsets.

V. Results

A. Spatial variance investigation

To match the results from model B with those from the measured data, the detector response distributions (presented in section III-A1) were convolved with a Gaussian distribution with a FWHM of 1.2 mm. This convolution incorporates any physical factors not modelled by the distributions, for example inter-crystal scatter, scintillation crosstalk, etc.

Figure 3 shows a comparison of the FWHM of each projection (view) of the simulated sinograms with those of the measured data. For a point source located near the centre of the FOV the FWHMs of the projections are quite constant, as expected. However, for off-centre point sources the FWHMs of the measured data vary with the projection angle, and this behaviour is well modelled by the redistribution technique (model B). Since the Gaussian convolution is spatially invariant, the FWHMs are not affected by the point source position and it thus underestimates the FWHM of the PSF for angles where the point source's projection is off-centre.

B. Static phantom scans

Figure 4 shows a slice through the reconstruction of the centred phantom using different resolution models. The reconstruction using the redistribution technique exhibits a very similar resolution recovery to the reconstruction using the Gaussian convolution, although it suffers from more noise. This is expected since the Gaussian model is accurate near the centre of the FOV.

Figure 5 shows a slice through the reconstruction of the off-centre phantom using different resolution models. The rods in the reconstruction using a Gaussian convolution have been slightly elongated in the horizontal direction due to the inaccurate modelling of the system response in this region

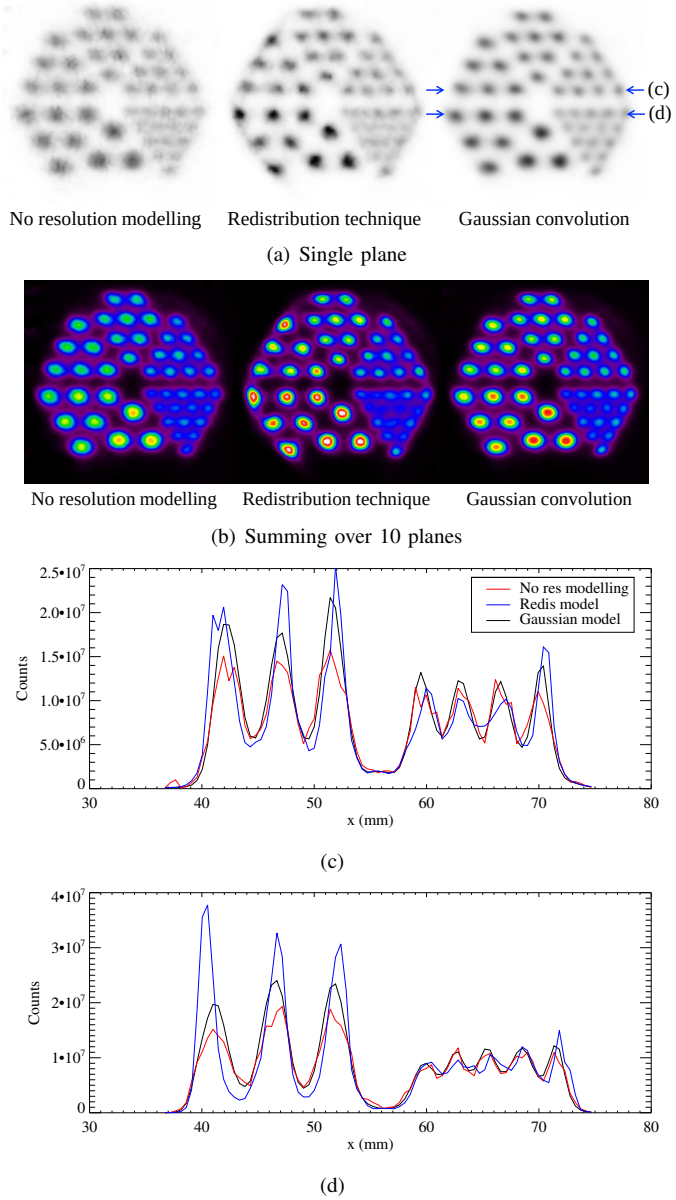

Fig. 5. Reconstructions of phantom 5.4 cm from the FOV centre. The Gaussian convolution method distorts the rods away from the centre (i.e. to the left), as can be seen in (b), while the redistribution technique has preserved the circular shape of the rods. The redistribution technique has produced a significant improvement in the resolution recovery.

of the FOV, while the reconstruction using the redistribution technique has preserved the circular shape of the rods. As can be seen in the profiles across the images in figure 5, the redistribution technique has produced better resolution recovery than the other two methods. However, it does suffer from noise introduced through the random redistribution of the LORs, and this has affected the resolution of the smallest rods.

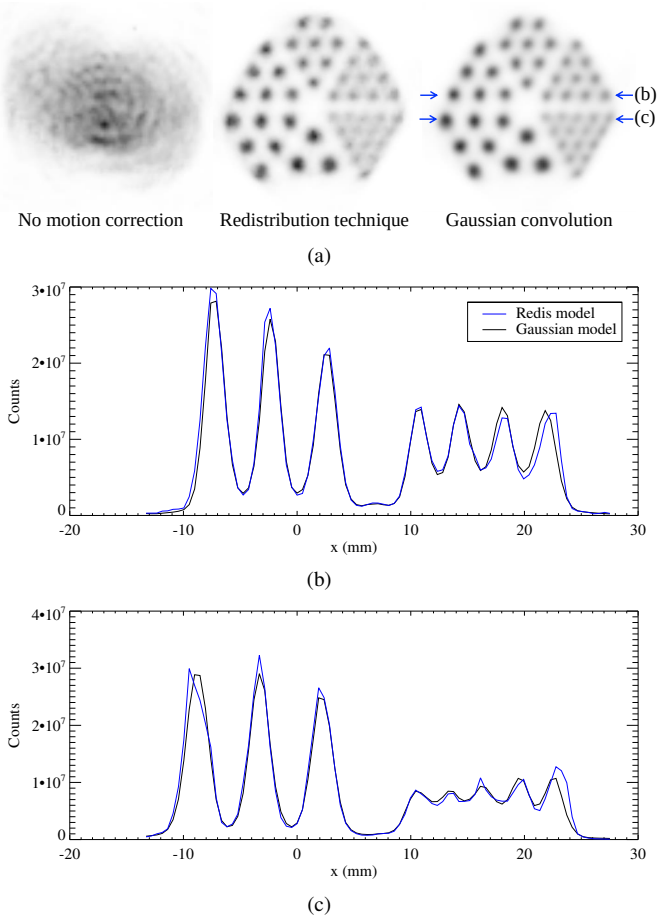

Fig. 6. Reconstruction of an off-centre, moving phantom. The redistribution technique shows a small but consistent improvement over the Gaussian convolution model.

C. Moving phantom scan

Figure 6 shows the results of the reconstruction of the moving phantom, compared to the reconstruction when using the Gaussian convolution technique to model the resolution. The profiles along two lines are also shown and while the improvement in the resolution recovery by the redistribution technique is small, it is consistent throughout the image.

VI. Discussion

Through an analytical modelling of the system response, the redistribution technique effectively models a tube-of-response for each detector pair, given sufficient sampling of the derived distributions. These tubes-of-response can overlap and vary radially, axially and transaxially. Since the LORs are redistributed randomly and at each sampling represent only a 1-dimensional sample of the 3-dimensional tube-of-response, a significant amount of noise is introduced into the MLEM reconstruction. This noise degrades the final resolution recovery. Nonetheless, since each LOR appears many times in the list-mode data (given a high enough number of counts), the TORs are sufficiently sampled to approximate the system response. The reading and redistribution of the LORs requires approximately 9 times more computation time than simply reading the LORs from file, and this needs to be performed twice at each iteration: once for the LORs for the forward projection and once for those for the backprojection. On most systems this amounts to a few minutes instead of a few seconds per sampling.

In the centre of the FOV the redistribution technique does not produce results any better than when using a Gaussian convolution model. This is expected since a Gaussian convolution is a good approximation to the system response near the centre of the FOV. Indeed, the resultant tube-of-response near the centre of the FOV when using the redistribution technique matches this Gaussian distribution closely. Since the redistribution technique involves a random sampling it introduces noise into the MLEM iterations and the effect of this noise is clear in the reconstructions. For this reason the Gaussian convolution produces superior reconstructions for centred phantoms. However, with increasing radial distance from the centre of the FOV the redistribution technique provides a better model for the system response than the Gaussian convolution model. This was well demonstrated by the sinogram simulated using the redistribution technique for an off-centre point source. In the case of the phantom data, at a distance of 5 cm from the FOV centre the Gaussian convolution noticeably elongates the reconstructed image radially away from the centre, while the redistribution technique preserves the shape of the imaged objects. Thus, even though there is an increase in the noise, it is nonetheless preferable to use the redistribution technique to model the resolution in these cases.

The redistribution technique is well-suited to be used in conjunction with motion correction. The LORs are redistributed before being motion corrected, and then used in the MLEM reconstruction, thus the spatial variance of the system response is preserved. The results of the moving phantom scan showed a small but consistent resolution recovery by the redistribution technique as compared to the Gaussian convolution method. The scale of this improvement may be explained by the fact that the phantom was not as far from the FOV centre as the presented static scans. A more eccentrically moving phantom may produce more pronounced results.

VII. Conclusion

A spatially variant resolution modelling technique has been presented which estimates the system matrix on-the-fly. The method randomly redistributes the LOR endpoints according to suitable probability density functions, then performs a list-mode OSEM reconstruction. An improved resolution was observed in off-centre phantom reconstructions when compared to the standard spatially invariant model of using a stationary Gaussian convolution in image space, however with an increase in noise. The technique was successfully applied to an event-by-event, list-mode motion correction reconstruction and a slight but consistent improvement in the resolution was observed.

REFERENCES

[1] S. E. Derenzo, "Mathematical Removal of Positron Range Blurring in High Resolution Tomography," *IEEE Trans. Nucl. Sci.*, vol. 33, no. 1, pp. 565–569, 1986.

[2] V. Y. Panin, F. Kehren, C. Michel, and M. Casey, "Fully 3-D PET reconstruction with system matrix derived from point source measurements." *IEEE Trans. Med. Imaging*, vol. 25, no. 7, pp. 907–21, Jul. 2006.

[3] A. M. Alessio, P. E. Kinahan, and T. K. Lewellen, "Modeling and incorporation of system response functions in 3-D whole body PET." *IEEE Trans. Med. Imaging*, vol. 25, no. 7, pp. 828–37, Jul. 2006.

[4] J. Qi, R. M. Leahy, S. R. Cherry, A. Chatziioannou, and T. H. Farquhar, "High-resolution 3D Bayesian image reconstruction using the microPET small-animal scanner." *Phys. Med. Biol.*, vol. 43, no. 4, pp. 1001–13, Apr. 1998.

[5] A. Reader, P. Julyan, H. Williams, D. Hastings, and J. Zweit, "EM Algorithm System Modeling by Image-Space Techniques for PET Reconstruction," *IEEE Trans. Nucl. Sci.*, vol. 50, no. 5, pp. 1392–1397, Oct. 2003.

[6] R. Siddon, "Fast calculation of the exact radiological path for a three-dimensional CT array," *Med. Phys.*, 1985.

[7] M. G. Bickell, A. Buffler, and I. Govender, "A fully 4D mesh parameterisation PET image reconstruction algorithm for list-mode data," *IEEE Nucl. Sci. Symp. Conf. Rec.*, pp. 2620–2624, Oct. 2011.

[8] A. J. Reader, S. Ally, F. Bakatselos, R. Manavaki, R. J. Walledge, A. P. Jeavons, P. J. Julyan, S. Zhao, D. L. Hastings, and J. Zweit, "One-Pass List-Mode EM Algorithm for Reconstruction Into Large Arrays," *IEEE Trans. Nucl. Sci.*, vol. 49, no. 3, pp. 693–699, 2002.

[9] S. Moehrs, M. Defrise, N. Belcari, A. D. Guerra, A. Bartoli, S. Fabbri, and G. Zanetti, "Multi-ray-based system matrix generation for 3D PET reconstruction." *Phys. Med. Biol.*, vol. 53, no. 23, pp. 6925–45, Dec. 2008.

[10] Y. Chen and S. J. Glick, "Determination of the System Matrix Used in List-Mode EM Reconstruction of PET," *IEEE Nucl. Sci. Symp. Conf. Rec.*, pp. 3855–3858, 2007.

[11] X. Jin, C. Chan, T. Mulnix, V. Panin, M. E. Casey, C. Liu, and R. E. Carson, "List-mode reconstruction for the Biograph mCT with physics modeling and event-by-event motion correction." *Phys. Med. Biol.*, vol. 58, no. 16, pp. 5567–5591, Jul. 2013.

[12] J. E. Gillam, P. Solevi, J. F. Oliver, and M. Rafecas, "Simulated one-pass list-mode: an approach to on-the-fly system matrix calculation." *Phys. Med. Biol.*, vol. 58, no. 7, pp. 2377–94, Apr. 2013.

[13] E. Gonzalez, J.-y. Cui, and G. Pratx, "Point spread function for PET detectors based on the probability density function of the line segment," *IEEE Nucl. Sci. Symp. Conf. Rec.*, vol. 1, pp. 4386–4389, 2011.

[14] A. Autret, J. Bert, O. Strauss, and D. Visvikis, "Fully 3D PET List-Mode reconstruction including an accurate detector modeling on GPU architecture," *Fully 3D 2013*, pp. 229 –232, 2013.

[15] X. Jin, C. Chan, and T. Mulnix, "List-mode reconstruction for the Biograph mCT with probabilistic line-of-response positioning and event-by-event motion correction," *IEEE Nucl. Sci. Symp. Conf. Rec.*, pp. 3682–3687, 2012.

[16] A. Z. Kyme, V. W. Zhou, S. R. Meikle, C. Baldock, and R. R. Fulton, "Optimised motion tracking for positron emission tomography studies of brain function in awake rats." *PLoS One*, vol. 6, no. 7, p. e21727, Jan. 2011.

[17] A. Rahmim, P. Bloomfield, S. Houle, M. Lenox, C. Michel, K. R. Buckley, T. J. Ruth, and V. Sossi, "Motion Compensation in Histogram-Mode and List-Mode EM Reconstructions : Beyond the Event-Driven Approach," *IEEE Trans. Nucl. Sci.*, vol. 51, no. 5, pp. 2588–2596, 2004.

[18] A. Kyme, S. Se, S. Meikle, C. Baldock, W. Ryder, and R. Fulton, "Novel SLAM-Based Markerless Motion Tracking of Conscious Unrestrained Rodents in PET," *IEEE Nucl. Sci. Symp. Conf. Rec.*, pp. 3554–3557, 2011.

[19] P. Noonan and T. Cootes, "The design and initial calibration of an optical tracking system using the Microsoft Kinect," *IEEE Nucl. Sci. Symp. Conf. Rec.*, pp. 3614–3617, 2011.

[20] R. Lecomte, D. Schmitt, and G. Lamoureux, "Geometry Study of a High Resolution PET Detection System Using Small Detectors," *IEEE Trans. Nucl. Sci.*, vol. NS-31, no. 1, pp. 556–561, 1984.

[21] Z. Liang, "Detector response restoration in image reconstruction of high resolution positron emission tomography." *IEEE Trans. Med. Imaging*, vol. 13, no. 2, pp. 314–21, Jan. 1994.

[22] D. Strul, R. B. Slates, M. Dahlbom, S. R. Cherry, and P. K. Marsden, "An improved analytical detector response function model for multi-layer small-diameter PET scanners." *Phys. Med. Biol.*, vol. 48, no. 8, pp. 979–94, Apr. 2003.

[23] P. Colombino, B. Fiscella, and L. Trossi, "Study of positronium in water and ice from 22 to -144 C by annihilation quanta measurements," *Nuovo Cim.*, vol. 38, pp. 707–23, 1965.

[24] K. Shibuya, E. Yoshida, F. Nishikido, T. Suzuki, T. Tsuda, N. Inadama, T. Yamaya, and H. Murayama, "Annihilation photon acollinearity in PET: volunteer and phantom FDG studies." *Phys. Med. Biol.*, vol. 52, no. 17, pp. 5249–61, Sep. 2007.

[25] S. Haber, S. Derenzo, and D. Uber, "Application of mathematical removal of positron range blurring in positron emission tomography," *IEEE Trans. Nucl. Sci.*, vol. 37, no. 3, pp. 1293–1299, Jun. 1990.

[26] Y.-C. Tai, A. Ruangma, D. Rowland, S. Siegel, D. F. Newport, P. L. Chow, and R. Laforest, "Performance evaluation of the microPET focus: a third-generation microPET scanner dedicated to animal imaging." *J. Nucl. Med.*, vol. 46, no. 3, pp. 455–63, Mar. 2005.